batteries

MDPI

Article

Thermal Safety Research of Lithium-Ion Batteries Based on Flame-Retardant Phase Change Materials

Jiaxin Zhang, Jiajun Zhao, Yin Chen * and Mingyi Chen *

School of the Environment and Safety Engineering, Jiangsu University, Zhenjiang 212013, China; 3210904015@stmail.ujs.edu.cn (J.Z.); zjj@stmail.ujs.edu.cn (J.Z.)
* Correspondence: chenyin@ujs.edu.cn (Y.C.); chenmy@ujs.edu.cn (M.C.)

Abstract: Pure phase change materials (PCMs) have drawbacks such as low thermal conductivity and poor physical properties like flammability, which limit their further application in battery thermal management systems. This paper introduces an innovative flame-retardant composite phase change material (CPCM) made from paraffin, expanded graphite, chitosan (CS), ammonium polyphosphate (APP), and aluminum hypophosphite (AHP). The physicochemical properties and flame-retardant performance of CPCMs with five different flame-retardant ratios of 9%, 12%, 15%, 18%, and 21% are studied, and their application effects in battery thermal safety are revealed. The results show that the combination of flame retardants CS, APP, and AHP exhibits effective synergistic effects, and the prepared CPCM exhibits good flame-retardant properties and thermal management effects. The CPCM exhibits outstanding thermal management performance when the flame-retardant content is 12%. At a maximum discharge rate of 3C, compared to natural air-cooling conditions, the maximum battery temperature and temperature difference are controlled within the safe range of 41 °C and below 5 °C, respectively. The CPCM can play an important role in the thermal safety of lithium-ion batteries.

Keywords: composite phase change materials; flame retardancy; battery thermal management

Academic Editor: Seiji Kumagai

Received: 2 January 2025
Revised: 22 January 2025
Accepted: 24 January 2025
Published: 26 January 2025

Citation: Zhang, J.; Zhao, J.; Chen, Y.; Chen, M. Thermal Safety Research of Lithium-Ion Batteries Based on Flame-Retardant Phase Change Materials. *Batteries* **2025**, *11*, 50. https://doi.org/10.3390/batteries11020050

1. Introduction

As global awareness of environmental protection intensifies, electric vehicles (EVs) and energy storage systems (ESSs) have garnered widespread attention due to their contributions to mitigating environmental pressures and natural resource shortages [1]. Lithium-ion batteries (LIBs) have emerged as the primary energy source in these fields, owing to their high energy density, long cycle life, and low self-discharge rates [2,3]. However, the thermal safety issues of LIBs, particularly the potential for performance degradation and safety risks under high-current operations, have always been a focus of industry concern [4]. LIBs generate significant amounts of heat during operation, and if this heat is not dissipated promptly, it may lead to thermal runaway (TR), resulting in serious consequences such as smoking, fires, or even explosions [5,6]. Therefore, an efficient battery thermal management system (BTMS) is crucial for ensuring the safe operation of LIBs. The BTMS aims to maintain battery temperatures within a safe range and control temperature variations at a reasonable level to optimize battery performance, capacity, and cycle life [7].

Conventional BTMS typically rely on methods like liquid cooling and air cooling [8,9], but these methods may not meet the cooling demands of high-energy-density LIBs in certain situations. Phase change materials (PCMs), as a passive cooling technology, have gradually become a research hotspot due to their high heat dissipation efficiency and the

absence of additional cooling power consumption [10,11]. PCMs can absorb and release a significant amount of heat during the phase change process, thereby effectively controlling battery temperatures. Previous researchers have carried out a lot of work on enhancing the thermal conductivity of PCM and have achieved good results, as shown in Table 1. The relationship between the base material and the content of thermal conductive additives on the performance of PCM (mainly thermal conductivity) is also relatively clear. These studies have laid the foundation for the development of PCM and its application in LIB thermal management.

Table 1. PCMs with enhanced thermal conductivity.

Basis Material	Thermally Conductive Additives	Effects	Reference
Paraffin (PA)	Multi-walled carbon nanotube (MWCNT) and activated carbon	39.1% and 34.1% increase in thermal conductivity	Sahan et al. [12]
PA	Graphene films	Enhanced the thermal conductivity to 11.594 W/m K	Yu et al. [13]
PEG	Carbon nanotubes (CNTs)	28.1% increase in thermal conductivity	Yan et al. [14]
PA	Expanded graphite (EG)	Thermal conductivity and latent heat reached 1.827 W/m K and 147.2 J/g	Zeng et al. [15]
PA	Copper nanoparticles	46.3% increase in thermal conductivity	Lin et al. [16]
PA	Organically modified montmorillonite (OMMT) and MWCNT	65% increase in thermal conductivity	Li et al. [17]
N-octadecane	Aerogel and borax cross-links	Thermal conductivity of 0.146 W/m K	Li et al. [18]
PA	Silicon carbide (SiC)/EG	Thermal conductivity is increased from 1.1 to 2.0 W/m K	Yuan et al. [19]
Myristic acid (MA), PA	Short carbon fibers (SCFs) and carbon black (CB)	Thermal conductivity of 8.7 W/m K	Li et al. [20]
PA	Graphite and coconut oil	Increased thermal conductivity from 0.2 W/m K to 15 W/m K	Wu et al. [21]
PA	EG and flaked copper powder	Thermal conductivity of 3.357 W/m K and latent heat of 137 J/g	Li et al. [22]
PA	EG	Thermal conductivity from 5.3 to 11.2 W/m K	Ling et al. [23]
PA	EG and MWCNT	Thermal conductivity of 2.23 W/m K	He et al. [24]

Our predecessors have made remarkable achievements in the preparation and application of CPCMs. Through a variety of innovative methods such as dispersion technology, ice template method, sol-gel method, melt mixing method, etc., a variety of high-performance CPCMs have been successfully prepared, which has significantly improved the thermal conductivity of PCM and effectively controlled electricity. When the discharge multiple was 3C, the maximum temperature of the battery based on the CPCM fabricated by Wang et al. remained within 46.5 °C, which was 34.2 °C lower compared to natural cooling [25]. Geng et al. prepared flexible CPCMs using PA as the PCM, styrene-ethylene/butylene-styrene block copolymer as the elastic carrier, and graphene as the thermal conductivity enhancer, and the highest temperature at the center of the LIB surface was reduced by 1.89 °C [26]. The maximum temperature of the battery module with CPCMs fabricated by Huang et al. could be controlled below 50 °C with 1C discharge, and the corresponding temperature difference effectively maintained within 2 °C [27]. Ma et al. designed a lauric acid (LA)/EG CPCM with a loading rate of up to 70% and a thermal conductivity of 2.546 W/(m·K), and the LIB temperature fluctuation was reduced by 45% [28]. Sun et al. prepared a CPCM based on PA/LA/EG, and the battery's maximum temperature decreased by 21 °C with 1C discharge [29]. To address the flammability of PA, Mei et al. proposed a CPCM with high heat absorption capacity. PA/SA (sodium acetate trihydrate) effectively delayed the temperature rise of the battery [30]. Cao et al. prepared a flexible CPCM with good retained flexibility, high electrical insulation, and thermal conductivity,

and the maximum temperature of the prismatic battery pack was controlled below 45 °C, with a temperature difference of 4 °C, even at a high discharge rate of 6C [31]. Kang et al. employed a novel high thermal conductivity CPCM made of PA and silicon to enhance heat transfer, which significantly narrowed the temperature range of the battery pack [32]. Yang et al. synthesized a novel CPCM with high resistivity and flexibility using natural rubber, and the operating temperature of the battery pack was maintained at 45 °C, with a temperature difference kept within 2 °C [33]. Deng et al. prepared a novel stable flexible CPCM, which exhibited good toughness and could control the battery temperature at 2 °C with a rate of 49.3 °C [34]. Yang et al. prepared a CPCM, which maintained a mass retention rate of over 99.9%, with the maximum temperature controlled at 44.7 °C and a temperature difference below 3.6 °C [35]. He et al. proposed a shape-stable CPCM based on metal–organic frameworks/EG/MWCNT, and the maximum temperature difference of the CPCM cooling module was 2.67 °C [24]. Fu et al. prepared a shape-stable and thermally induced flexible CPCM with binary alkanes, and the temperature of LIBs was reduced by 3.42 °C to 16.41 °C at discharge rates of 1–3C [36]. However, the application of PCM also faces challenges, such as the flammability of organic PCM at high temperatures. However, although these achievements are excellent in thermal management, they still need to be further strengthened in flame-retardant inhibition. Although some studies, such as those investigating the use of modified glass fiber, have tried to enhance the flame retardancy of CPCM, overall, how to better suppress the flammability of CPCM while improving the efficiency of thermal management is still a problem that needs to be solved in the future research.

The core objective of this research is to develop a PCM that possesses an appropriate melting temperature range, exceptional latent heat storage capacity, and superior flame retardancy to efficiently absorb heat generated during battery operation. This study specifically focuses on PA-based PCMs because of their exceptionally high latent heat storage capacity within a narrow melting temperature range. However, despite PA's sufficient energy storage density, it suffers from low thermal conductivity and it is highly flammable. Ammonium polyphosphate (APP), as an efficient halogen-free flame-retardant, can effectively reduce the burning speed of materials, and decrease the production of smoke and toxic gases. Chitosan (CS), a renewable natural polymer material, can serve as a char-forming agent, promoting the isolation of oxygen and preventing the spread of flames. Aluminum hypophosphite (AHP) is an inorganic flame-retardant with low smoke production and excellent flame-retardant properties. To overcome these challenges, we have incorporated EG to improve thermal conductivity and added flame-retardant powders to enhance both thermal conduction and flame resistance. Additionally, this study explores the potential of flame-retardant batteries in BTMS by comparing their thermal management performance at various discharge rates.

2. Materials and Methods

2.1. Material Preparation

Firstly, the flame retardant is prepared by mixing APP, CS, and AHP in a mass ratio of 2:2:1 until uniform. Secondly, a certain amount of PA is placed in a beaker, and the beaker containing the PA is placed in an oven at 90 °C for 30 min until it melts. Then, the beaker containing the PA is placed in a magnetic stirrer with the temperature set to 90 °C. A flame retardant with a mass ratio of x (x = 0, 9, 12, 15, 18, 21%) is added and stirred for 30 min to ensure uniform mixing of the PA and flame retardant. Subsequently, EG with a mass ratio of 5% is added and stirred for another 30 min to ensure uniform mixing of the PA, flame retardant, and EG. Finally, the prepared flame-retardant CPCM is cooled at room

temperature and pressed into a mold. Figure 1 illustrates the preparation method of the samples. Table 2 shows the composition of the flame-retardant CPCM.

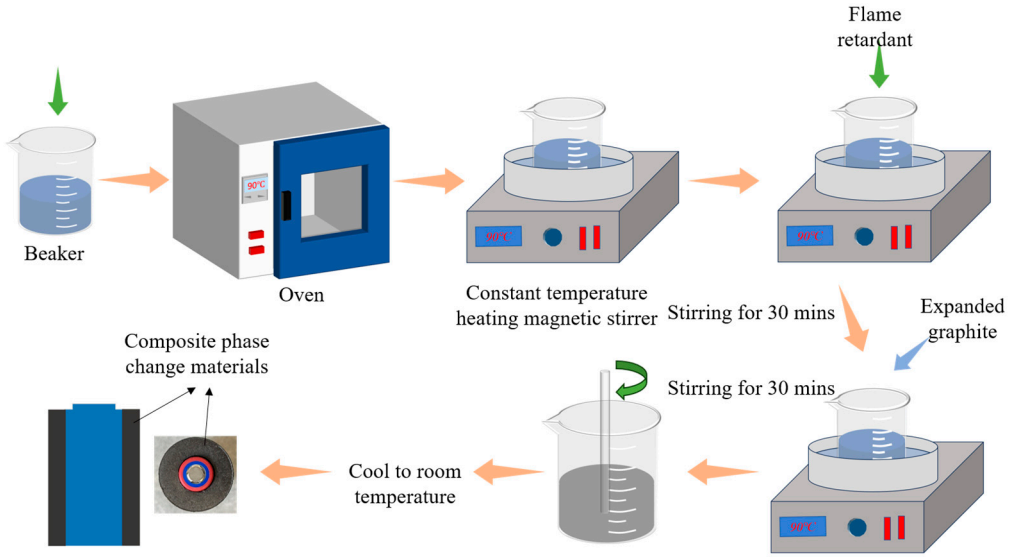

Figure 1. Synthesis diagram of the flame-retardant CPCMs.

Table 2. Mass content of the flame-retardant CPCMs.

Sample	Mass Content (wt%)		
	PA	EG	APP/CS/AHP
M1	95	5	0
M2	86	5	9
M3	83	5	12
M4	80	5	15
M5	77	5	18
M6	74	5	21

2.2. Material Properties

2.2.1. Chemical Properties and Thermophysical Properties

The thermal conductivity of the prepared flame-retardant CPCM samples was measured using the Xiangtan DRE-III (Xiangtan Xiangyi Instrument Co., Ltd., Xiangtan, China) Multifunctional Rapid Thermal Conductivity Tester. The prepared samples were cylinders with a radius of 40 mm and a height of more than 8 mm. To reduce errors, 2–3 preliminary tests were performed before each formal test to ensure the thermal conductivity of the samples stabilized. The average value was obtained from five measurements for each sample. The microstructure and compositional distribution of the prepared flame-retardant CPCM were examined using a Hitachi Regulus-8100 (HITACHI, Tokyo, Japan) Field Emission Scanning Electron Microscope. The phase change temperature and latent heat of the flame-retardant CPCM were measured using a Mettler-Toledo DSC3 Differential Scanning Calorimeter (NETZSCH Scientific Instruments Trading Ltd., Selb, German) under a nitrogen atmosphere, with a temperature range of 30 to 90 °C and a heating rate of 10 °C/min.

2.2.2. Flame-Retardant Performance

The flame-retardant CPCM was pressed into a mold with a size of 79 mm × 14 mm × 10 mm. The horizontal combustion melting experiment under normal air atmosphere was carried out, and the samples were clamped with a clip. A combustion expansion experiment was conducted on the foam copper plate. After the sample was ignited, a HDR-

CX405 camera (Sony, Japan) was used to record the changes before and after combustion of flame-retardant CPCMs.

2.3. Battery Thermal Management Experimental Settings

In this experiment, the prepared flame-retardant CPCM was applied to a single battery to study its thermal management performance. An 18650 LIB with a nominal capacity of 3.4 Ah, an actual capacity of 3.2 Ah, a rated voltage of 3.7 V, and a fully charged voltage of 4.2 V was used. The battery was initialized through cycling and left to stand for more than 24 h to ensure normal operation and provide a consistent starting point for subsequent testing of the battery during cycling. In this experiment, a thermocouple was connected to the middle of the battery for temperature measurement.

Figure 2 shows the construction of the experimental platform and the arrangement of the thermocouples. The entire system includes a thermostat providing an ambient temperature of 25 °C; a battery charge–discharge cycling instrument for charging and discharging the battery; an Agilent data acquisition module for collecting battery temperature data and uploading it to a computer terminal; and a computer terminal for recording the temperature data. The synthesized PCMs containing different proportions of flame retardants were pressed into ring shapes with a thickness of 16.5 cm using a mold and superimposed onto the 18650 single cell battery to ensure that the battery casing was completely encapsulated by the PCM. The single-cell battery was charged and discharged both in the air and while wrapped in M1-M6, with discharge rates set in two groups (2C and 3C) and a charge rate of 1C. The specific operating conditions are shown in Table 3. In this experiment, to avoid accidents, each set of experiments was repeated at least twice, and the average values of the two experimental data sets were analyzed.

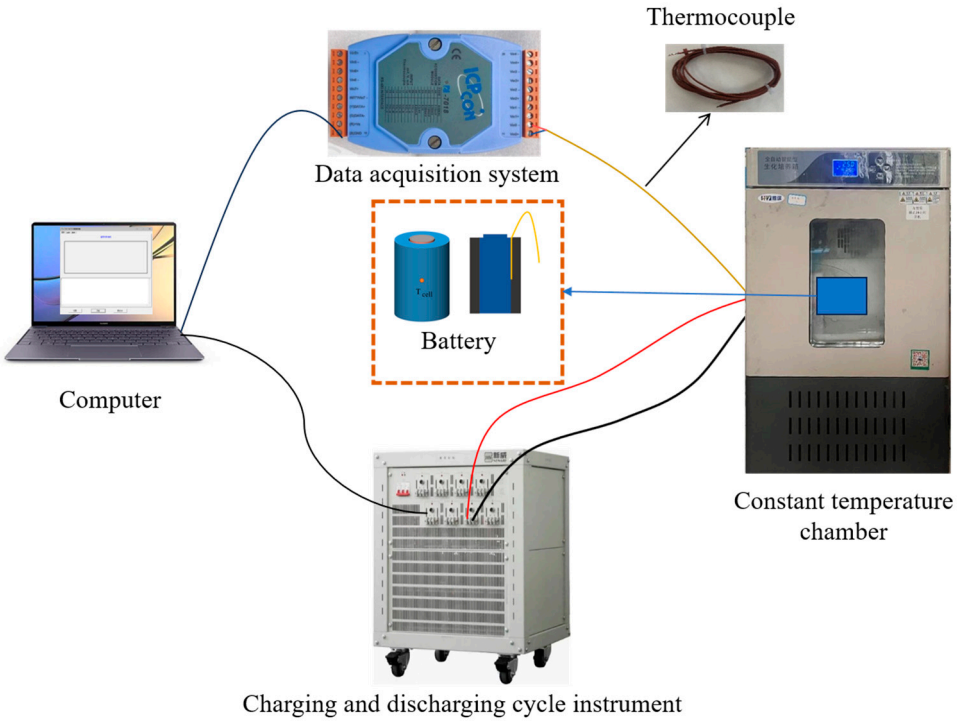

Figure 2. Battery charge and discharge experimental test platform.

Table 3. Design parameters of experimental working conditions.

Process Settings	Battery Status
Standby	Ten mins
Constant current discharging	Discharge cut-off voltage at 2.75 V, currents of 6.4 A (2C) and 9.6 A (3C)
Standby	Ten mins
Constant current and pressure charging	4.2 V and 3.2 A
Cycling numbers	Two

3. Results and Discussion

3.1. Characteristics of Flame-Retardant CPCMs

The SEM images presented in Figure 3 offer visual proof of the surface characteristics of various materials, including EG, CS, AHP, APP, and CPCMs M1–M6 with differing fire-retardant ratios. Figure 3a–c reveals the presence of numerous irregular and distinctive worm-like microporous structures within the EG, accompanied by a rough surface texture. These unique structures serve as attachment points for wax and fire retardants, facilitating their integration.

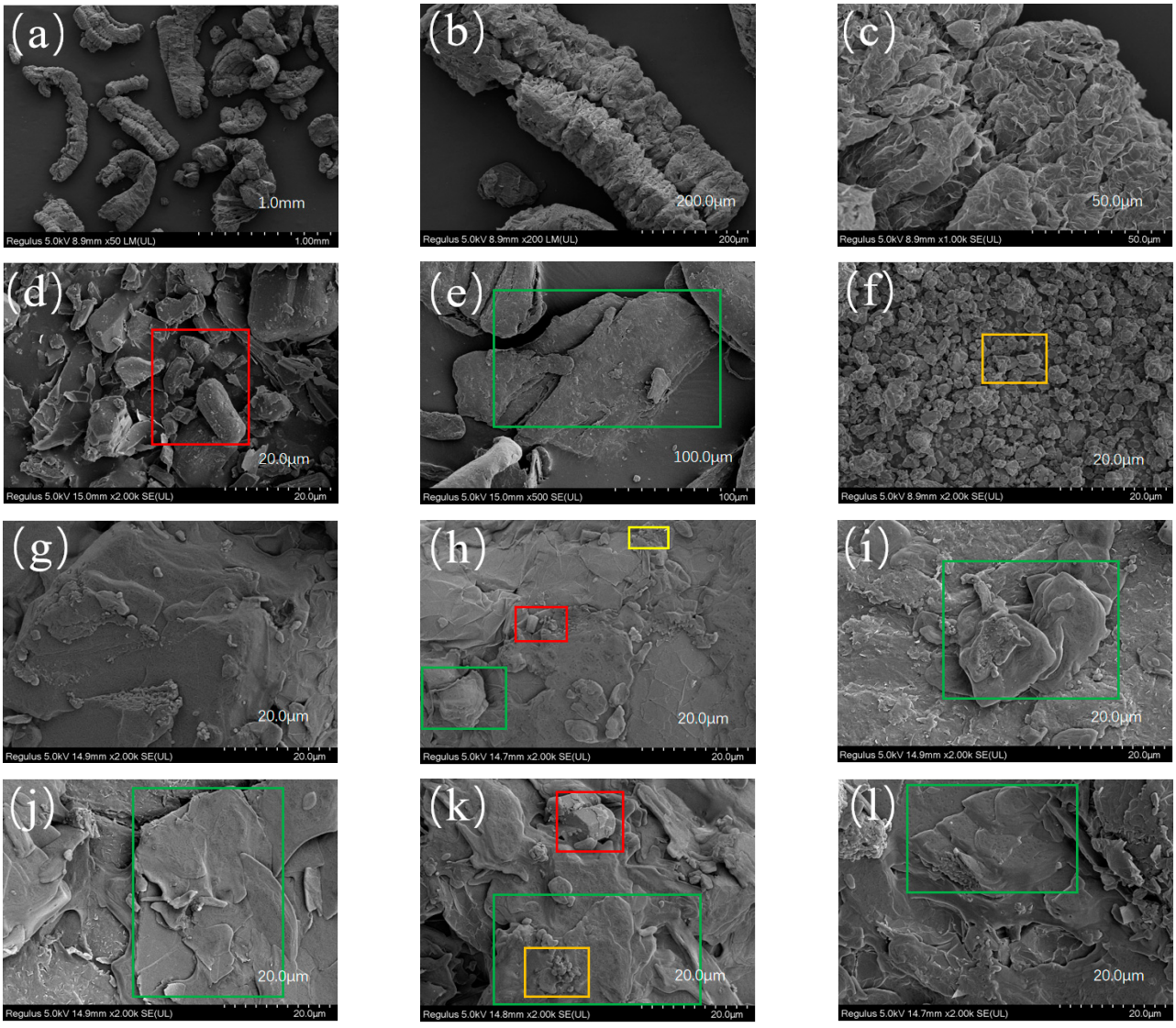

Figure 3. SEM morphology (**a**–**c**) EG; (**d**) APP; (**e**) AHP; (**f**) CS; (**g**) M1; (**h**) M2; (**i**) M3; (**j**) M4; (**k**) M5; (**l**) M6.

In Figure 3d–f, we observe the fire retardant containing columnar, platelet-like, and crystalline granular structures. These diverse morphological features contribute to the fire retardant's effectiveness. Figure 3g demonstrates the successful adsorption of wax onto the microporous structures of the EG, resulting in a surface that is relatively smooth and even when the wax and EG are combined.

Furthermore, Figure 3h–l showcases the successful integration of wax and fire retardant with the microporous structures of the EG. A portion of the fire retardant penetrates into the interior of the EG, while the remainder adheres to its surface. This interaction transforms the initially smooth and even surface into a rougher one. As the concentration of the fire retardant increases, so does the degree of surface roughness.

In summary, the structural insights derived from the SEM images suggest that the integration of wax, fire retardants, and EG results in a material with enhanced thermal conductivity and improved overall performance. The increased surface roughness and the interaction between the fire retardants and the EG not only optimize the material's fire resistance but also contribute to more efficient heat dissipation. This enhancement in thermal properties, combined with the material's ability to effectively absorb and distribute heat, makes it a promising candidate for use in battery thermal management systems. By improving the thermal conductivity and stability under high temperatures, this CPCM is well suited to maintain optimal operating conditions in energy storage devices, thereby promoting safety and efficiency in battery performance.

The XRD results are shown in Figure 4. PA exhibits significant diffraction peaks at 21.71° and 23.83°, while EG shows a peak at 26.59°. AHP has diffraction peaks at 15.39°, 16.12°, and 26.17°, and APP displays a peak at 15.59°. Notably, M1 shows the same diffraction angles as PA, EG, APP, and AHP, with no additional peaks. Similarly, M1–M6 all display diffraction peaks at the same 2θ values. However, as the PA ratio decreases, the peaks at 21.45° and 23.77° gradually weaken. This can be attributed to the dispersion of granular IFR in PA, which impacts the crystallinity of PEG. Importantly, no new diffraction peaks were observed for any of the CPCMs, indicating that the synthesis of the PCM involved only physical mixing, with no chemical reactions occurring.

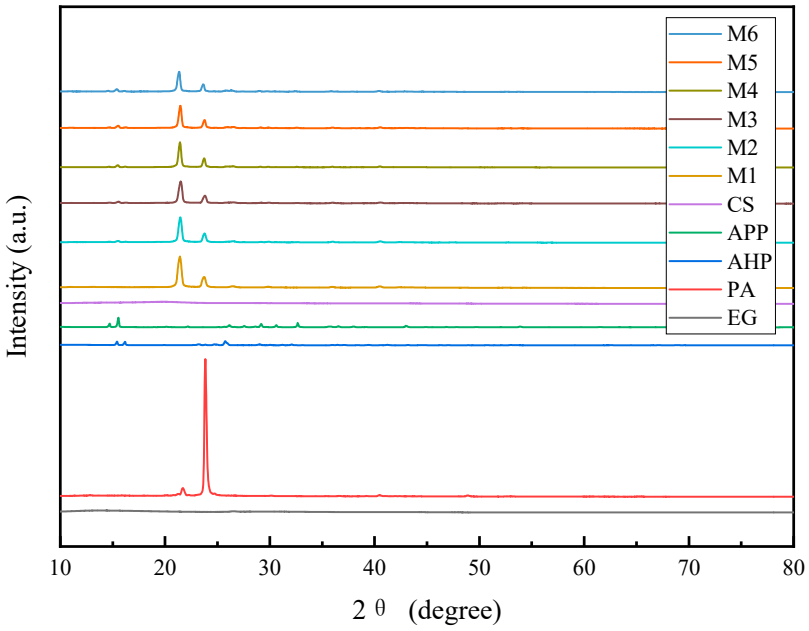

Figure 4. XRD patterns of different samples.

Figure 5 presents the results of thermal conductivity tests conducted on flame-retardant CPCMs. The thermal conductivity of a material is crucial in determining its ability to absorb and dissipate thermal energy. Enhancing thermal conductivity allows for more efficient absorption and dissipation of thermal energy while reducing thermal gradients and improving temperature uniformity within the PCM, thereby enhancing the stability of its thermal performance. This experiment investigated the changes in thermal conductivity across different material ratios, with the thermal conductivity coefficients of PA and M1–M6 being 0.2, 1.2, 1.18, 1.16, 1.14, 1.12, and 1.1 W/m K, respectively. Compared to PA, the addition of EG to PA results in a six-fold increase in thermal conductivity compared to pure PA. This increase in thermal conductivity is primarily attributed to the EG. The worm-like structure of EG interconnects to form a thermal conductivity framework, with PA adhering to the pores of the EG, thereby enhancing the thermal conductivity of M1. Furthermore, upon adding varying proportions of flame retardants, a slight decrease in the thermal conductivity of the flame-retardant CPCMs was observed. This reduction is attributed to the lower thermal conductivity of the added flame retardants compared to pure PA [37,38]. The thermal conductivity of APP is generally between 0.1 and 0.3 W/m K, and the thermal conductivity of CS is 0.185 W/m K, which is lower compared with PA with 0.2 W/m K. In general, as the proportion of flame retardant added increases, the thermal conductivity of CPCMs gradually decreases.

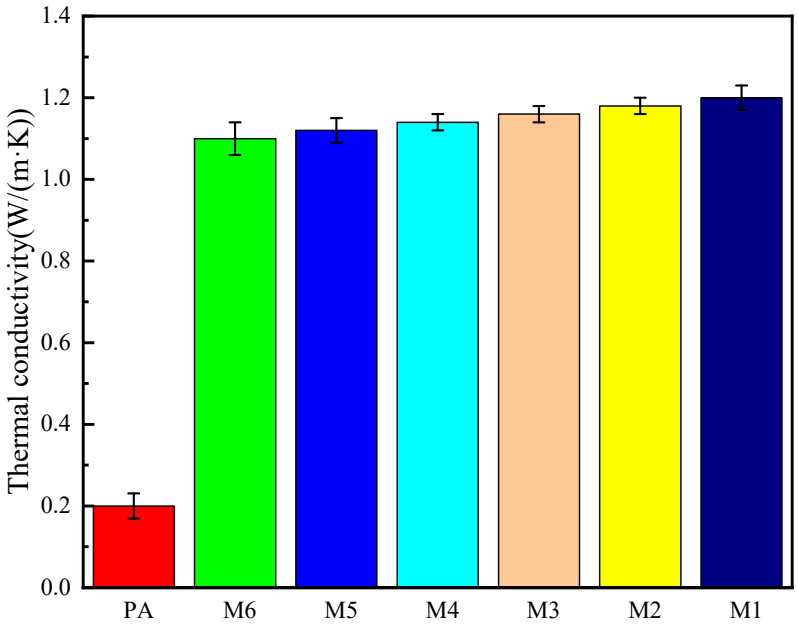

Figure 5. Thermal conductivity of different CPCM samples.

The DSC curves of PA and CPCMs M1–M6 are depicted in Figure 6, and the thermophysical parameters are shown in Table 4. The results indicate that the introduction of thermally conductive filler EG and a flame retardant reduces the latent heat of the PCMs. The peak phase change temperature of PA is observed at 45.34 °C, corresponding to a maximum latent heat of 227.45 J/g. Upon the addition of 5% EG, the peak temperature of M1 decreases to 45.27 °C, with a maximum latent heat of 192.61 J/g. Further incorporation of flame retardant into this base results in a decrease in latent heat from 179.78 J/g for M2 to 133.72 J/g for M6, accompanied by a reduction in peak temperature from 45.33 °C to 44.67 °C. These findings suggest that the latent heat of the flame-retardant CPCMs is primarily determined by the proportion of PA. A lower percentage of PA leads to a decrease in the latent heat of the flame-retardant CPCMs [37,38]. The incorporation of a flame

retardant slightly lowers the peak temperature of the materials. Overall, the incorporation of EG and flame retardants improves the thermal conductivity of the materials, facilitating a faster heat transfer. As a result, the materials undergo continuous melting and release latent heat at lower temperatures, leading to a reduction in peak temperature.

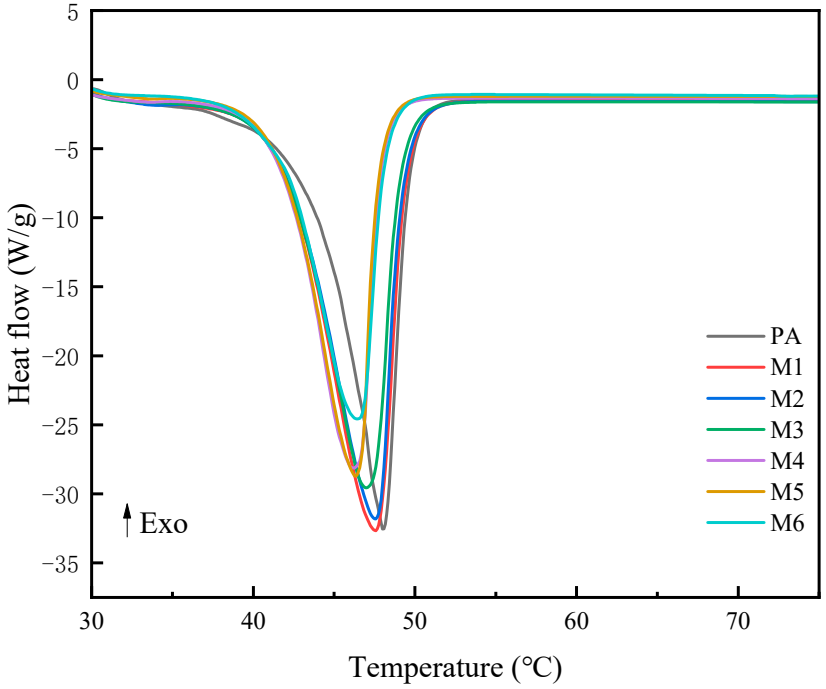

Figure 6. DSC curves for various CPCM samples.

Table 4. Thermophysical parameters of PCMs.

Samples	Peak Phase Change Temperature (°C)	Latent Heat of Phase Change ΔH (J/g)
PA	45.34	227.45
M1	45.27	192.61
M2	45.33	179.78
M3	44.91	165.87
M4	44.26	149.40
M5	44.30	163.75
M6	44.67	133.72

3.2. Flammability Test of Flame-Retardant Composite Phase Change Materials

The photograph in Figure 7 depicts the before and after images of suspended horizontal combustion melting experiment and fusing of flame-retardant CPCMs with varying flame-retardant contents. Prior to the addition of any flame retardant, the fusing time for M1 was 300 s. However, upon incorporating flame retardants, the fusing times for M2 to M6 were recorded as 66 s, 59.5 s, 100.5 s, 94.5 s, and 65 s, respectively. These data reveal a trend: as the proportion of flame-retardant increases, the fusing time of the samples initially decreases, then increases, and finally decreases again. The rationale behind this phenomenon lies in the gradual increase in material density with the addition of flame retardants. Due to variations in material distribution uniformity and the influence of gravity, the fusing time decreases. When the flame-retardant addition reaches 15%, the fusing time begins to decrease once more, indicating that the incorporation of flame retardants can significantly reduce the fusing time of CPCMs. In fact, the fusing time can be shortened by up to 4.61 times with the optimal flame-retardant content.

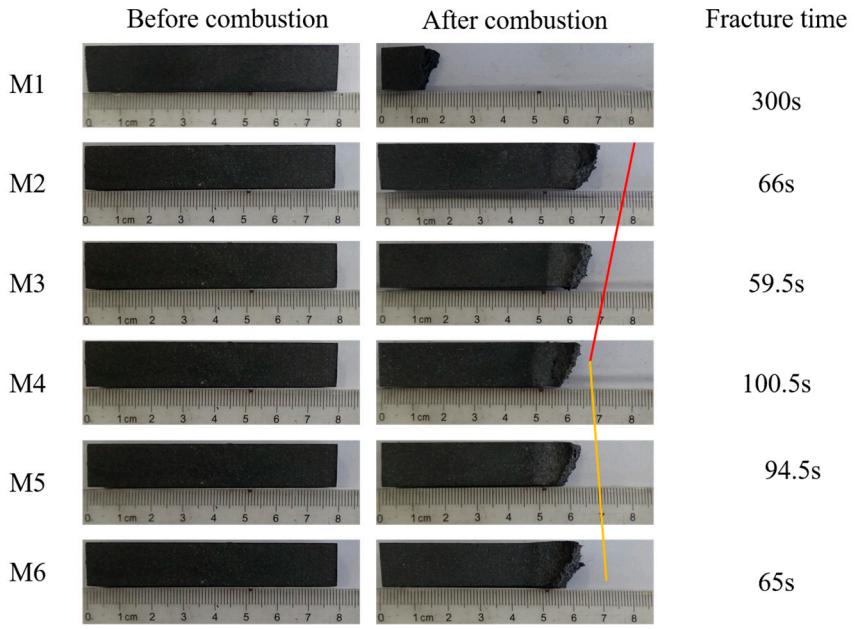

Figure 7. Horizontal combustion melting experiment residue of samples.

Figure 8a illustrates the varying degrees of expansion observed in CPCMs with different flame-retardant contents after undergoing burning tests. Specifically, when the mass ratio of the flame retardant is 12%, the composite material M3 expands by 6 mm compared to M1. As an intumescent flame retardant, APP undergoes thermal decomposition during the burning of the flame-retardant CPCM. The resulting ammonia and water cause the volume of the material to increase, forming a closed, porous, and fluffy carbonized layer on its surface. This layer hinders heat conduction within the PCM and blocks the flow of oxygen from the external environment to the surface of the flame-retardant composite. Figure 8b presents the extinguishment times recorded during burning tests of flame-retardant CPCMs with varying flame-retardant contents. It shows that as the proportion of the flame retardant in the composite increases, the total burning time of M1 to M6 decreases continuously. When the mass ratio of the flame retardant is 18%, M4 exhibits a significant reduction of 368 s compared to M5, demonstrating remarkable improvements in flame retardancy. By comparing the flame morphologies during the burning process of composites with different flame-retardant proportions, it is evident that the flame during the burning of M5 is smaller. This is due to the high flammability of PA, where an insufficient amount of flame retardant fails to effectively suppress the flame. However, when the flame-retardant content increases to 18%, it exhibits excellent flame control capabilities. The CS/APP/AHP in the flame retardant exhibits effective synergistic effects. The flame-retardant CPCM prepared with these components promotes the carbonization of the substrate, forming a dense, continuous, and expanded carbon layer on the surface, which inhibits the transfer of heat and oxygen [39–41]. The nitrogen (N) element present in CS and APP flame retardants plays a crucial role in inhibiting combustion. When heated, these substances decompose to release a significant amount of non-combustible gases, such as N_2, NH_3, and CO_2, which reduce the oxygen concentration and dilute the flammable gases in the combustion zone. This process contributes to the flame-retardant effect. APP, in particular, provides an acid source that acts as a dehydration agent. During thermal degradation, it produces phosphoric acid and polyphosphoric acid, which help promote the formation of a dense carbon layer at higher temperatures. The CS serves as a gas source and functions as a foaming agent. This foaming action expands the flame-retardant system and encourages the formation of a porous foam carbon layer, which further aids in flame suppression.

Due to the insufficient supply of oxygen and thermal energy, the burning flame-retardant CPCM will eventually extinguish. When the flame-retardant content reaches 18%, the duration of the burning process of the flame-retardant CPCM continues to shorten, but the reduction in time is weakened by 3.5 times compared to M6. The most significant flame suppression effect is achieved at this flame-retardant dosage. There is a balance between the flame-retardant properties, thermal stability, mechanical properties, thermal conductivity and battery thermal management applications of the CPCMs. Adding an appropriate amount of flame retardant can effectively improve the flame-retardant properties of the CPCMs, delay the combustion process and enhance thermal stability. However, excessive addition of flame retardants may lead to a decrease in the thermal conductivity of the CPCMs and may reduce the mechanical properties and thermal management application value. Therefore, a flame retardant with high flame-retardant efficacy at lower dosages is required [42,43].

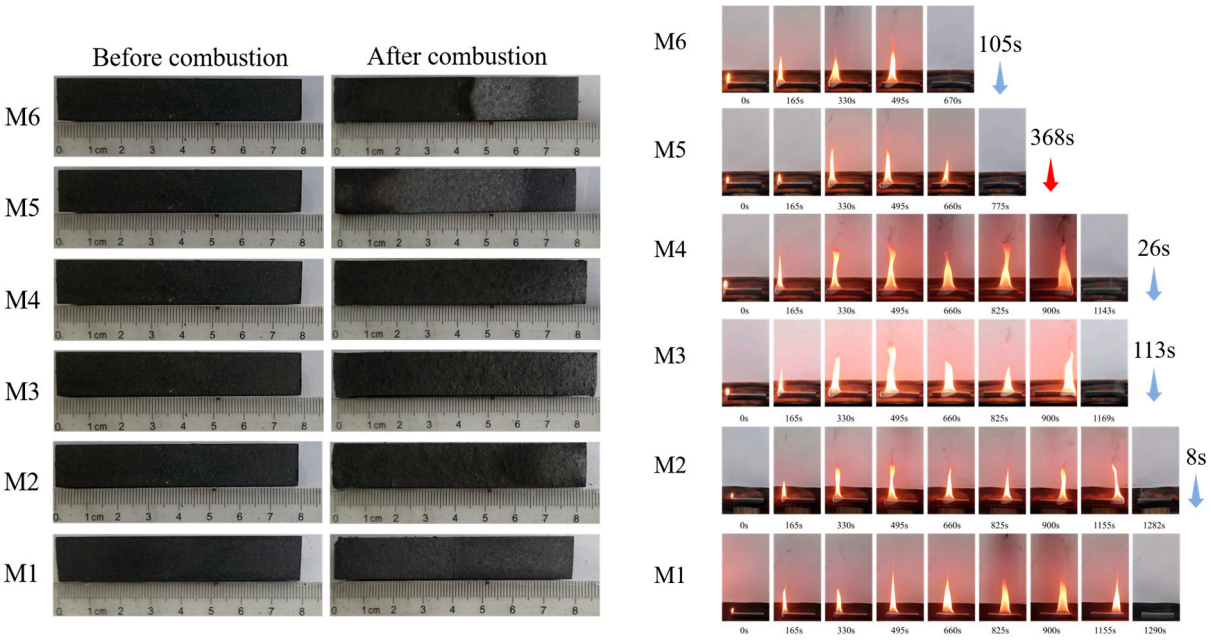

(**a**) Morphological features (**b**) Combustion process

Figure 8. Horizontal combustion expansion photos of different CPCMs placed on barbed wire.

3.3. Thermal Management Characteristics of Monomer Batteries

Temperature plays a significant role in the overall performance of batteries. In practical applications, it is crucial to comprehensively consider the effects of temperature on battery performance, lifespan, and safety. During the charging and discharging cycles of lithium-ion batteries, heat is generated due to reversible reactions, ohmic resistance, polarization effects, and side reactions within the battery. When the heat produced exceeds the battery's heat dissipation capacity, it manifests as an increase in battery temperature. The generation of heat in batteries is primarily influenced by their internal resistance and the magnitude of the charging and discharging currents. The faster the charging and discharging rates, the quicker the battery temperature rises. To assess the effect of flame-retardant CPCMs with varying flame-retardant contents on battery thermal management performance, this experiment examined the cooling effects of six types of flame-retardant CPCMs and natural air cooling. Figure 9a,b illustrates the charging and discharging temperature curves of batteries under different operating conditions, specifically at 2C and 3C rates. The maximum battery temperatures are shown in Figure 10. When batteries undergo charging and discharging cycles at 2C and 3C rates under natural air cooling, the maximum temperatures

reached are 46.2 °C and 59.0 °C, respectively. This indicates that under natural air cooling, batteries are unable to quickly transfer the generated heat to the external environment during charging and discharging cycles, leading to heat accumulation within the battery. The flame-retardant CPCMs act as a buffer during battery charging and discharging cycles, absorbing heat as the battery temperature increases and releasing heat when it decreases. At a 3C rate, the thermal management performance of CPCMs is significantly superior to that of natural air cooling. Under high-rate discharge currents, the maximum battery temperature exceeds the phase transition temperature of the flame-retardant CPCMs, allowing the latent heat to be fully utilized. Compared to natural air cooling, the use of M3 results in a maximum temperature of 40.9 °C, a reduction of 18.1 °C. At a 2C discharge rate, the thermal management performance of flame-retardant CPCMs varies with the proportion of flame retardant. When the flame-retardant content is 12%, it exhibits excellent thermal management performance, reducing the maximum battery temperature to 38 °C, a decrease of 8.2 °C compared to natural air cooling. However, as the flame-retardant content continues to increase, the thermal management performance of the flame-retardant CPCMs deteriorates, which can be attributed to the reduction in thermal conductivity and latent heat of the materials caused by the increased flame-retardant content.

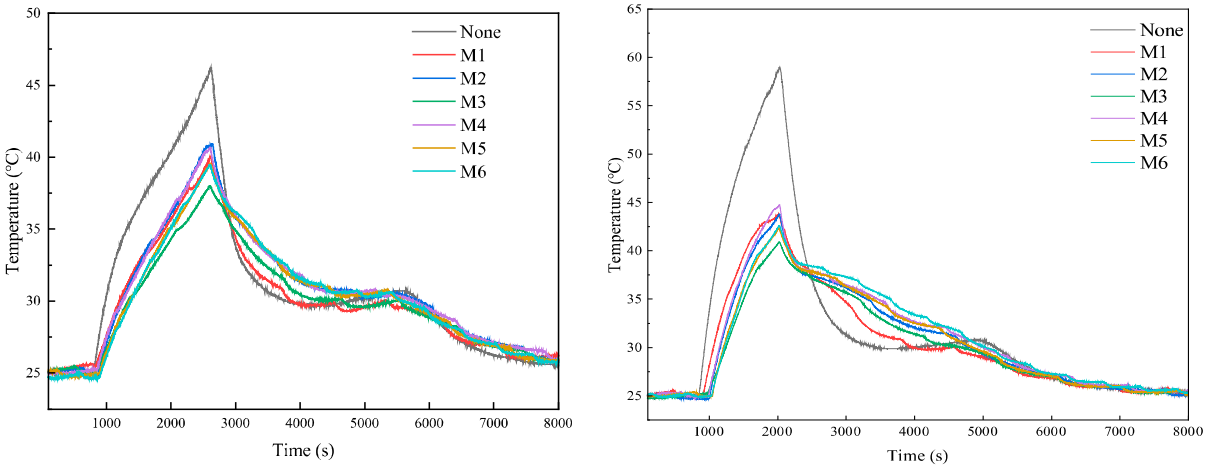

(**a**) 2C (**b**) 3C

Figure 9. Cell temperature curve with different samples at 2C and 3C rates.

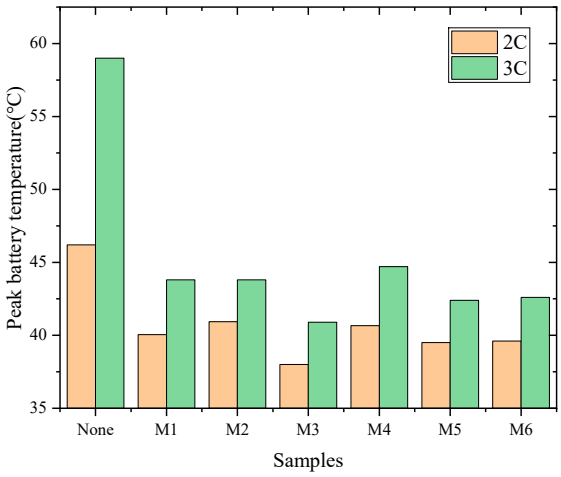

Figure 10. The maximum battery temperatures with different samples at 2C and 3C rates.

4. Conclusions

This work successfully developed a novel flame-retardant CPCM composed of PA, CS, APP, and AHP through the melt blending method. This study focused on investigating its impact on the thermal safety characteristics of lithium-ion batteries. The research findings indicate that the addition of 12% flame retardant significantly enhances the fusing performance of the flame-retardant CPCM. When the flame-retardant content reaches 18%, the material demonstrates exceptional flame control capabilities. This is attributed to the effective combination of CS, APP, and AHP with PA and EG, which improves the dense carbon layer of the material, thereby enhancing its thermal insulation and oxygen barrier properties. Furthermore, in battery thermal management applications, the flame-retardant CPCM exhibits outstanding thermal management effects. Especially when the flame-retardant content is appropriately balanced, the battery's temperature can be maintained below 41 °C under 3C discharge conditions, representing a 31.4% reduction in temperature compared to natural air cooling. However, as the flame-retardant content increases, the overall heat storage capacity of the material must meet the demands of battery thermal management; otherwise, it may compromise its thermal management performance.

Author Contributions: Methodology, Y.C.; Investigation, J.Z. (Jiaxin Zhang); Data curation, J.Z. (Jiajun Zhao); Writing—original draft, J.Z. (Jiaxin Zhang) and J.Z. (Jiajun Zhao); Writing—review & editing, J.Z. (Jiaxin Zhang), J.Z. (Jiajun Zhao), Y.C. and M.C.; Supervision, M.C. All authors have read and agreed to the published version of the manuscript.

Funding: This research received no external funding.

Data Availability Statement: The original contributions presented in the study are included in the article, further inquiries can be directed to the corresponding author.

Conflicts of Interest: The authors declare no conflict of interest.

References

1. Song, X.; Deng, C.; Shen, P.; Qian, Y.; Xie, M. Environmental Impact and Carbon Footprint Analysis of Pure Electric Vehicles Based on Life Cycle Assessment. *Res. Environ. Sci.* **2023**, *36*, 2179–2188.
2. Hu, L.; Tian, Q.; Huang, J.; Ye, Y.; Wu, X. Review on Energy Distribution and Parameter Matching of Lithium-ion Battery-super Capacitor Hybrid Energy Storage System for Electric Vehicles. *J. Mech. Eng.* **2022**, *58*, 224–237.
3. Wu, K.; Zhang, Y.; Zeng, Y.Q.; Yang, J. Safety Performance of Lithium-Ion Battery. *Prog. Chem.* **2011**, *23*, 401–409.
4. Xu, D.; Li, Q.; Qiao, Q.; Xiao, W.; Yan, J.; Li, Y. Research progress of high-safety lithium-ion battery separators. *New Chem. Mater.* **2023**, *51*, 40–44.
5. Li, C.; Tang, X.; Wei, Z. Thermal runaway and prevention of lithium-ion batteries. *Sci. Technol. Rev.* **2024**, *42*, 178–192.
6. Hu, G.; Liao, C.; Zhang, W. A review on thermal runaway of lithium-ion batteries for electric vehicle. *Adv. Technol. Electr. Eng. Energy* **2021**, *40*, 66–80.
7. Patel, J.R.; Rathod, M.K. Recent developments in the passive and hybrid thermal management techniques of lithium -ion batteries. *J. Power Sources* **2020**, *480*, 27. [CrossRef]
8. Yang, C.Y.; Xi, H.; Wang, M.W. Structure optimization of air cooling battery thermal management system based on lithium-ion battery. *J. Energy Storage* **2023**, *59*, 22. [CrossRef]
9. Lu, M.Y.; Zhang, X.L.; Ji, J.; Xu, X.F.; Zhang, Y.Y.C. Research progress on power battery cooling technology for electric vehicles. *J. Energy Storage* **2020**, *27*, 16. [CrossRef]
10. Cai, S.W.; Zhang, X.L.; Ji, J. Recent advances in phase change materials-based battery thermal management systems for electric vehicles. *J. Energy Storage* **2023**, *72*, 27. [CrossRef]
11. Chen, J.W.; Kang, S.Y.; Jiaqiang, E.; Huang, Z.H.; Wei, K.X.; Zhang, B.; Zhu, H.; Deng, Y.W.; Zhang, F.; Liao, G.L. Effects of different phase change material thermal management strategies on the cooling performance of the power lithium ion batteries: A review. *J. Power Sources* **2019**, *442*, 18. [CrossRef]
12. Sahan, N.; Fois, M.; Paksoy, H. The effects of various carbon derivative additives on the thermal properties of paraffin as a phase change material. *Int. J. Energy Res.* **2016**, *40*, 198–206. [CrossRef]

13. Yu, J.; Kong, L.; Wang, H.Q.; Zhu, H.J.; Zhu, Q.S.; Su, J.W. A Novel Structure for Heat Transfer Enhancement in Phase Change Composite: Rolled Graphene Film Embedded in Graphene Foam. *ACS Appl. Energy Mater.* **2019**, *2*, 1192–1198. [CrossRef]
14. Yan, D.; Cai, W.; Yin, G.; Tang, B.; Zhang, S. Preparation and properties of PEG/APS-SiO_2/O-CNTs phase change materials with enhanced thermal conductivity. *Fine Chem.* **2021**, *38*, 729–735.
15. Jin, A.; Ju, Y.; Sun, H.; Li, H.; Zhang, Z. Mechanical properties of filling materials containing composite phase change materials. *J. Cent. S. Univ. Sci. Technol.* **2021**, *52*, 3153–3163.
16. Lin, S.C.; Al-Kayiem, H.H. Evaluation of copper nanoparticles—Paraffin wax compositions for solar thermal energy storage. *Sol. Energy* **2016**, *132*, 267–278. [CrossRef]
17. Li, M.; Guo, Q.G.; Nutt, S. Carbon nanotube/paraffin/montmorillonite composite phase change material for thermal energy storage. *Sol. Energy* **2017**, *146*, 1–7. [CrossRef] [PubMed]
18. Li, Z.C.; Zhang, Y.; Cao, F.; Yang, C.X.; Wang, X.; Zhang, S.F.; Tang, B.T. Poly(vinyl alcohol)-Based Composite Aerogel Phase-Change Material for Thermal Management. *ACS Appl. Energy Mater.* **2024**, *7*, 3009–3017. [CrossRef]
19. Yuan, W.Z.; Yang, X.Q.; Zhang, G.Q.; Li, X.X. A thermal conductive composite phase change material with enhanced volume resistivity by introducing silicon carbide for battery thermal management. *Appl. Therm. Eng.* **2018**, *144*, 551–557. [CrossRef]
20. Li, J.H.; Huang, J.H.; Liu, Z.Q.; Cao, M.; Chen, R.K.; Zhang, Y.F. Developing ternary composite phase change materials with two different phase change temperatures for battery thermal management. *Appl. Therm. Eng.* **2023**, *227*, 13. [CrossRef]
21. Upadhyay, D.; Mujadia, V.; Daruwala, R.; Lakdawala, A.; Shah, D.V. Investigation on performance of composite phase change material based thermal management of electrical battery. *Int. J. Interact. Des. Manuf. Ijidem* **2024**, *18*, 4285–4294. [CrossRef]
22. Li, J.H.; Huang, J.H.; Zhai, Q.; Zhen, Y.Q.; Liu, Z.Q.; Zhang, Y.F. A novel flexible composite phase change material applied to the thermal safety of lithium-ion batteries. *J. Energy Storage* **2024**, *86*, 14. [CrossRef]
23. Ling, Z.; Chen, J.; Fang, X.; Zhang, Z.; Xu, T.; Gao, X.; Wang, S. Experimental and numerical investigation of the application of phase change materials in a simulative power batteries thermal management system. *Appl. Energy* **2014**, *121*, 104–113. [CrossRef]
24. He, R.; Fang, M.; Zhou, J.; Fei, H.; Yang, K. Enhancement of battery thermal management effect by a novel MOF based composite phase change material. *Appl. Therm. Eng.* **2024**, *257*, 124257. [CrossRef]
25. Wang, H.; Li, J.; Li, W. Thermal management of lithium-ion batteries based on PA/OBC/EG composite phase change materials. *New Chem. Mater.* **2022**, *50*, 141.
26. Geng, Y.; Li, J.; Zhang, Y. Simulation study on the effect of flexible composite phase change materials for thermal management of lithium-ion batteries. *New Chem. Mater.* **2024**, *52*, 187–192.
27. Huang, Q.Q.; Li, X.X.; Zhang, G.Q.; Kan, Y.C.; Li, C.B.; Deng, J.; Wang, C.H. Flexible composite phase change material with anti-leakage and anti-vibration properties for battery thermal management. *Appl. Energy* **2022**, *309*, 15. [CrossRef]
28. Ma, Y.; Yang, H.; Zuo, H.Y.; Zuo, Q.S.; He, X.X.; Chen, W.; Wei, R.R. EG@Bi-MOF derived porous carbon/lauric acid composite phase change materials for thermal management of batteries. *Energy* **2023**, *272*, 10. [CrossRef]
29. Sun, Y.; Zhang, G.; Chen, K.; Dou, B. Temperature Control Performance of Soft-Coated Lithium-Ion Battery Based on Paraffin/Lauric Acid/Expanded Graphite. *Adv. New Renew. Energy* **2023**, *11*, 457–463.
30. Mei, J.; Shi, G.Q.; Liu, H.; Wang, Z. Organic and Inorganic Hybrid Composite Phase Change Material for Inhibiting the Thermal Runaway of Lithium-Ion Batteries. *Batteries* **2023**, *9*, 14. [CrossRef]
31. Cao, J.H.; Ling, Z.Y.; Lin, X.M.; Wu, Y.; Fang, X.M.; Zhang, Z.G. Flexible composite phase change material with enhanced thermophysical, dielectric, and mechanical properties for battery thermal management. *J. Energy Storage* **2022**, *52*, 13. [CrossRef]
32. Kang, W.; Zhao, Y.Q.; Jia, X.H.; Hao, L.; Dang, L.P.; Wei, H.Y. Paraffin/SiC as a Novel Composite Phase-Change Material for a Lithium-Ion Battery Thermal Management System. *Trans. Tianjin Univ.* **2021**, *27*, 55–63. [CrossRef]
33. Yang, K.X.; Ling, Z.Y.; Fang, X.M.; Zhang, Z.G. Introducing a flexible insulation network to the expanded graphite-based composite phase change material to enhance dielectric and mechanical properties for battery thermal management. *J. Energy Storage* **2023**, *66*, 11. [CrossRef]
34. Deng, Q.; Liu, Q.; Nian, Y.L.; Zhao, R.; Cheng, W.L. A novel flexible composite phase change material with enhanced toughness and shape stability for battery thermal management. *J. Energy Storage* **2023**, *72*, 14. [CrossRef]
35. Yang, W.S.; Li, X.X.; Li, C.B.; Deng, J.; Du, Y.X.; Zhang, G.Q. High Antileakage and Thermal Conductivity Composite Phase-Change Material with Anisotropy Expanded Graphite for Battery Thermal Management. *ACS Appl. Energy Mater.* **2023**, *6*, 9698–9708. [CrossRef]
36. Fu, L.Y.; Wu, Z.X.; Wu, K.Y.; Chen, W.D.; Zhang, M.M.; Huang, X.; Ma, C.; Shao, Y.L.; Ran, J.Y.; Chua, K.J. A thermally induced flexible composite phase change material with boron nitride nanosheets/carbon nanotubes modified skeleton for battery thermal management. *Appl. Energy* **2024**, *373*, 13. [CrossRef]
37. Gong, Y.; Zhang, J.; Chen, Y.; Ouyang, D.; Chen, M. Application of Polyethylene Glycol-Based Flame-Retardant Phase Change Materials in the Thermal Management of Lithium-Ion Batteries. *Polymers* **2023**, *15*, 4450. [CrossRef]
38. Zhao, L.; Yan, H.-q.; Fang, Z.-p. Flame Retardancy of Ramie Fabrics Treated by Layer-by-layer Assembly Technique of Tri-component PEI/PAA/APP. *Acta Polym. Sin.* **2017**, 982–989. [CrossRef]

39. Qiu, H.; Zhang, Z.; Ling, Z.; Fang, X. Developing a flame-retardant flexible composite phase change material to realize both temperature control and thermal runaway prevention for lithium-ion battery pack. *Appl. Therm. Eng.* **2024**, *248*, 123301. [CrossRef]
40. Liu, Q.; Deng, Q.; Zhao, R.; Cheng, W.-L.; Wang, Y.-D. A novel flexible flame-retardant phase change materials with battery thermal management test. *J. Energy Storage* **2023**, *70*, 108077. [CrossRef]
41. Niu, J.; Deng, S.; Gao, X.; Niu, H.; Fang, Y.; Zhang, Z. Experimental study on low thermal conductive and flame retardant phase change composite material for mitigating battery thermal runaway propagation. *J. Energy Storage* **2022**, *47*, 103557. [CrossRef]
42. Liu, M.; Qiao, J.; Zhang, X.; Guo, Z.; Liu, X.; Lin, F.; Yang, M.; Fan, J.; Wu, X.; Huang, Z. Flame Retardant Strategies and Applications of Organic Phase Change Materials: A Review. *Adv. Funct. Mater.* **2025**, *35*, 2412492. [CrossRef]
43. Pielichowska, K.; Paprota, N.; Pielichowski, K. Fire Retardant Phase Change Materials—Recent Developments and Future Perspectives. *Materials* **2023**, *16*, 4391. [CrossRef] [PubMed]